Kinetics of DNA-mediated docking reactions between vesicles tethered to supported lipid bilayers

Yee-Hung M. Chan*, Peter Lenz†, and Steven G. Boxer*‡

*Department of Chemistry, Stanford University, Stanford, CA 94305; and †Department of Physics, Philipps-University Marburg, Renthof 5, D-35032 Marburg, Germany

Edited by Jacob N. Israelachvili, University of California, Santa Barbara, CA, and approved October 8, 2007 (received for review June 28, 2007)

Membrane–membrane recognition and binding are crucial in many biological processes. We report an approach to studying the dynamics of such reactions by using DNA-tethered vesicles as a general scaffold for displaying membrane components. This system was used to characterize the docking reaction between two populations of tethered vesicles that display complementary DNA. Deposition of vesicles onto a supported lipid bilayer was performed by using a microfluidic device to prevent mixing of the vesicles in bulk during sample preparation. Once tethered onto the surface, vesicles mixed via two-dimensional diffusion. DNA-mediated docking of two reacting vesicles results in their colocalization after collision and their subsequent tandem motion. Individual docking events and population kinetics were observed via epifluorescence microscopy. A lattice-diffusion simulation was implemented to extract from experimental data the probability, P_{dock}, that a collision leads to docking. For individual vesicles displaying small numbers of docking DNA, P_{dock} shows a first-order relationship with copy number as well as a strong dependence on the DNA sequence. Both trends are explained by a model that includes both tethered vesicle diffusion on the supported bilayer and docking DNA diffusion over each vesicle's surface. These results provide the basis for the application of tethered vesicles to study other membrane reactions including protein-mediated docking and fusion.

Many biological processes involve tightly regulated interactions between two membrane surfaces. These typically are initiated by the recognition and binding of complementary molecules displayed on the two membrane surfaces. Examples include cell adhesion (1), signaling cascades as in the case of the immunological T cell response (2), and neuronal fusion, where synaptic vesicles first dock to the presynaptic membrane, then undergo lipid mixing and content release (3). Studying the kinetics of binding reactions can give insights into competitive binding, the sequence of assembly of protein complexes, and other biological problems. The complexity of these reactions has led to the development of model membrane systems allowing better control over reaction components and conditions. In the case of vesicle fusion, many model experiments have been performed by using artificial vesicles, which can be reacted in three dimensions (4–6) or to supported bilayers (7–9). In the case of cell adhesion and the T cell response, supported lipid bilayers displaying some of the relevant components have been used to mimic at least one of the cell surfaces (10). Here, we employ a hybrid system in which small (≈50-nm radius) unilamellar vesicles are tethered to a fluid supported bilayer (11, 12) to probe individual vesicle–vesicle collisions and reactions.

Supported lipid bilayers are formed by vesicle fusion to appropriate substrates (13). Many methods now are available for controlling the organization (patterning) and composition of supported bilayers (14). However, it has proved much more difficult to reconstitute membrane-associated proteins into supported lipid bilayers because of unfavorable interactions with the underlying solid support, which can lead to loss of protein lateral mobility and function. Various strategies have been described to preserve these aspects by assembling the bilayer on softer materials (15–17) or tethering it to a hard surface (18, 19) with mixed success. Membrane proteins are routinely isolated by using detergents and transferred into lipid vesicles. Individual vesicles generally are studied after confining them either by adsorption directly onto a surface (20), in which case interactions with the surface again create problems, or by more gently attaching the vesicle to a surface by a tether. If a supported lipid bilayer first is assembled on a surface, further nonspecific vesicle interactions with the surface are minimized. When tethering ligands such as biotin (21–24) or a DNA oligonucleotide (11, 12, 25) are displayed on the supported bilayer, then individual intact vesicles displaying the complementary receptor can be held close to the surface where they can be visualized. Biotin-streptavidin tethers have been used extensively to isolate individual vesicles primarily in the context of single-molecule fluorescence measurements (21, 24). In our experience, such tethered vesicles are relatively immobile on the surface, which is ideal for single-molecule measurements but less useful for probing interactions between tethered vesicles.

Lipid molecules with short DNA oligonucleotides (typically 24-mer) replacing the head group can be used to tether vesicles as illustrated in Fig. 1. These vesicles diffuse in two dimensions, parallel to the plane of the supporting bilayer. The average diffusion constant, $\langle D_{ves} \rangle$, for these tethered vesicles typically is about five times less than that of fluorophore labeled lipids (26). Although diffusing parallel to the plane of the supporting bilayer, tethered vesicles collide reversibly with one another. In earlier work, we showed that collisions between vesicles containing negatively charged lipids resulted in transient associations in the presence of Ca ions because of chelate effects (12). Here, we investigate the probability that vesicles displaying complementary DNA sequences dock, that is, collide and do not separate but continue to diffuse together (see Fig. 1).

Results

Deposition of Vesicles Using a Microfluidic Device. Vesicles displaying complementary DNA sequences dock in solution faster than they tether to the supported lipid bilayer. Thus, it is necessary to keep the vesicle solutions separated during tethering to prevent premature mixing and docking of vesicles before imaging of the surface begins. Earlier work by Kam and Boxer showed the utility of using microfluidic devices to create composition variations across supported bilayers (27, 28). Thus, to prevent mixing during tethering, a three-lane flow channel was fashioned out of a polydimethylsiloxane (PDMS) device attached to a glass substrate (Fig. 2*A*). A supported bilayer is formed across the entire channel surface by vesicle fusion displaying tethering sequence A or B everywhere. (Table 1 lists complete sequences of all DNA used in this study.)

Author contributions: Y.-H.M.C., P.L., and S.G.B. designed research; Y.-H.M.C. and P.L. performed research; Y.-H.M.C. and P.L. contributed new reagents/analytic tools; Y.-H.M.C. analyzed data; and Y.-H.M.C., P.L., and S.G.B. wrote the paper.

The authors declare no conflict of interest.

This article is a PNAS Direct Submission.

‡To whom correspondence should be addressed at: Department of Chemistry, Stanford University, 380 Roth Way, Stanford, CA 94305. E-mail: sboxer@stanford.edu.

This article contains supporting information online at www.pnas.org/cgi/content/full/0706114104/DC1.

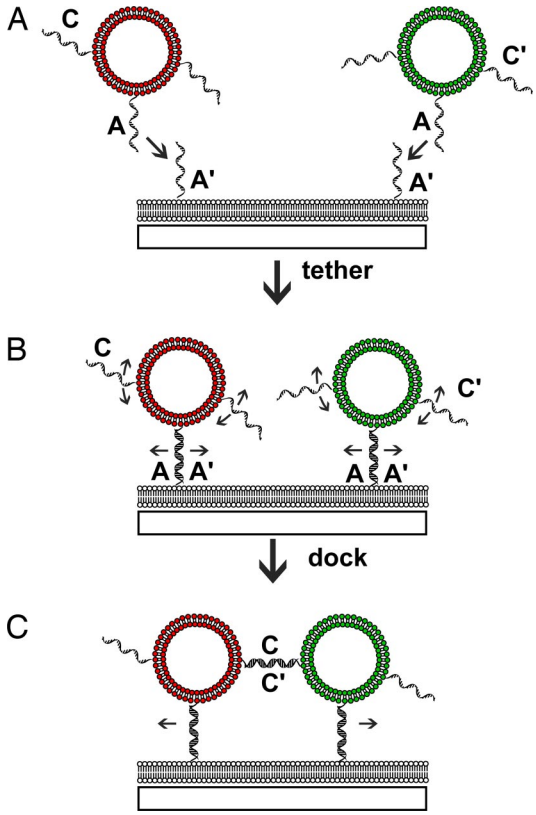

Fig. 1. Graphical illustration of vesicles being tethered to a supported bilayer and subsequent DNA-mediated docking between tethered vesicles. (*A*) Vesicles with a tethering DNA (sequence A) and docking DNA (sequence C or C′) are incubated with a supported bilayer that displays the complementary tethering DNA (sequence A′). (*B*) Hybridization of A and A′ tethers the vesicles to the supporting bilayer, and the vesicles are free to diffuse in the plane of the supported bilayer. Tethered vesicle diffusion and diffusion of the docking DNA on the vesicles' surfaces are illustrated with arrows. (*C*) Collisions between vesicles can lead to docking of tethered vesicles via hybridization of C and C′ DNA.

Then during the tethering process, two populations of vesicles are flowed in the two outer lanes while buffer without any vesicles is flowed in the central lane. Flow within the channel is laminar, so only diffusive mixing occurs, which is sufficient to keep vesicles in the outer lanes from appreciably mixing and docking across the central lane. A three-stripe pattern forms on the supported bilayer: two outer stripes of tethered vesicles separated by a middle area that is largely free of tethered vesicles (Fig. 2*B*). Once deposited, the two populations of tethered vesicles diffuse, become increasingly mixed over time, collide, and, in some cases, dock.

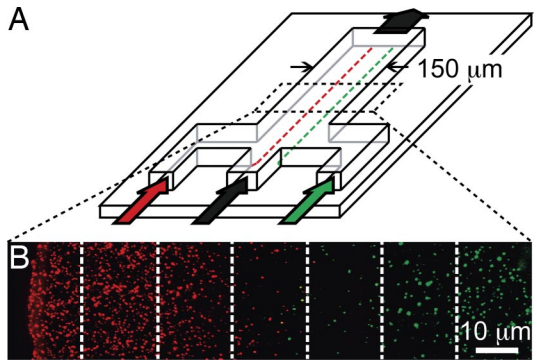

Fig. 2. Vesicle deposition using a microfluidic device. (*A*) Schematic of the device. The red and green lines mark the three lanes of flow created by the three inputs. (*B*) Composite image of the initial locations of OG and TR vesicles on the right and left sides, respectively, of a flow channel. The cross-sectional image was compiled from seven videos taken to span the deposition area.

Real-Time Imaging of DNA-Mediated Docking and Analysis of Diffusion. Vesicles labeled with Oregon green (OG) and Texas red (TR) displaying an average of 10 oligos with sequences D and D′, respectively, were deposited with the microfluidic device. As these vesicles diffused toward the center of the channel, some of the movies taken show collisions between OG and TR vesicles, many of which did not result in colocalization. However, several resulted in the docking of the vesicle pair, as illustrated in Fig. 3 and supporting information (SI) Movie 1. (Such events have been observed rarely because of the intermittent visualization of the sample necessitated by considerations including photostability.) Before colliding, the vesicles diffuse with no correlation between the two trajectories. Then they collide in frame 61, after which the red and green signals remain colocalized for the remainder of the video. Interestingly, the vesicles do not stop diffusing but continue to move in tandem, which is what is expected if the D/D′ DNA has successfully hybridized, connecting the OG and TR vesicles. Otherwise, they would continue to exhibit random motion with respect to each other after the collision. All three pairs of docking DNA sequences studied were capable of mediating docking. In contrast to the transient, calcium-mediated aggregation of tethered vesicles labeled with phosphatidylserine (12), DNA-docked pairs do not separate over the time scale of 1 h. Docking is not observed between tethered vesicle populations labeled with noncomplementary DNA strands.

Because of their spectral overlap, OG and TR dyes can participate in Förster resonant energy transfer (FRET). In these experiments, FRET would result in the quenching of OG (donor) emission simultaneous with an increase in TR (acceptor) emission. This concerted change in emission intensities was not observed during any of the movies taken. This finding implies that lipid mixing between vesicles does not occur. Furthermore, if the docking DNA is perpendicularly oriented to the vesicles' surface, as is likely based on previous results (29), the vesicles would be held ≈8 nm apart, so little intervesicle FRET is expected because most dyes are farther than this distance from each other on the two surfaces.

Kinetic Analysis of DNA-Mediated Docking. To determine the kinetics of DNA-mediated interactions of tethered vesicles, a series of videos was taken starting immediately after deposition was finished, then at 10-min intervals for up to 1 h. For each time point, enough videos were taken to create an image of the cross-section of the channel. Colocalized vesicles moving in tandem were identified as docked vesicle pairs and were counted as the total number of docking reactions that had occurred. This counting method assumes that the reverse rate of docking and the rate of multiple docking events are negligible on the time scale of observation, both of which are consistent with observation.

Fig. 4*A* shows the time courses from three kinetic trials where OG and TR vesicles present an average of 10 copies of DNA with sequences D and D′, respectively. These vesicles were deposited in a flow channel in separated populations and allowed to mix. The initial time points include a nonzero number of docked vesicles, which may have reacted in bulk because of imperfect separation in the flow channel. However, subsequent reactions must involve pairs of tethered vesicles, because all excess vesicles in bulk are removed by washing before observation. The linear trend is typical of these experiments, and the slope gives an effective rate describing the DNA-mediated docking reaction between tethered vesicles. Because the tethering process does not place vesicles in identical locations, the initial positions and densities of vesicles differ from trial to trial. Thus, each experiment produces a different time

Table 1. Sequences of tethering (A/A′ and B/B′) and docking (C/C′, D/D′, and E/E′) DNA used in DNA–lipid conjugates

DNA	Sequence
Tethering	
A	5′-TGCGGATAACAATTTCACACAGGA-3′
A′	5′-TCCTGTGTGAAATTGTTATCCGCA-3′
B	5′-TAACTACAGAATTTATACTATCCCGGGTCACAGCAGAGAAACAAGATA-3′
B′	5′-TATCTTGTTTCTCTGCTGTGACCCGGGATAGTATAAATTCTGTAGTTA-3′
Docking	
C	5′-TAGTATTCAACATTTCCGTGTCGA-3′
C′	5′-TCGACACGGAAATGTTGAATACTA-3′
D	5′-AAAAAAAAAAAAAAAAAAAAAAAA-3′
D′	5′-TTTTTTTTTTTTTTTTTTTTTTTT-3′
E	5′-TTTTTTTTTTTTTTTTTTTTTTTTTTTTAGTATTCAACATTTCCGTGTCGA-3′
E′	5′-TTTTTTTTTTTTTTTTTTTTTTTTTTTTCGACACGGAAATGTTGAATACTA-3′

All sequences are coupled to the lipophilic tail group on the 5′-end.

course and effective rate, even though the vesicles used are from the same preparation.

The usual methods for extracting a rate constant from these experimental time courses do not apply here because conventional bimolecular kinetics derivations assume homogeneous mixing of the two reactants in a defined area or volume. This is not true with these samples (or, in fact, for most membrane–membrane interactions), where mixing of tethered vesicles occurs very slowly compared with the reaction being observed, and the distribution of vesicles across the channel is inhomogeneous and evolves over the course of the experiment. Furthermore, each vesicle deposition gives rise to a different number of vesicles tethered and their initial position in the channel.

To extract kinetic information that can be compared between different experiments, we used a square-lattice diffusion model of the experiment to realistically simulate the diffusion-reaction problem. The initial placement of vesicles is taken from the observed cross-section of the first time point in the experimental trial. When the simulation is run, vesicles undergo a random walk in two dimensions that leads to mixing, collisions, and docking. The experimentally observed average tethered vesicle diffusion constant $\langle D_{ves} \rangle$ defines the relationship between the lattice spacing and the simulation time scale. The only independently specified parameter in the simulation is the probability, P_{dock}, that a collision between a red and green vesicle will result in a docking event. The number of docked vesicles is counted with respect to time, and plots of the output generally show linear trends that are consistent with experiments (Fig. 4*B*).

Because each simulation evolves randomly, 10 simulation trials were run for each set of initial conditions—vesicle coordinates, diffusivity, and P_{dock} value—to give a representative set of time courses. The time courses were fit to linear trends whose slopes were averaged to give a representative simulated rate. This process was repeated for several P_{dock} values, and that value which produces a representative simulated rate matching the experimental rate was taken to describe the docking reactivity of vesicle populations in that experimental trial. Fig. 4*B* shows a plot of the simulation output using vesicle coordinates from trial 1 in Fig. 4*A* (squares). Thirty

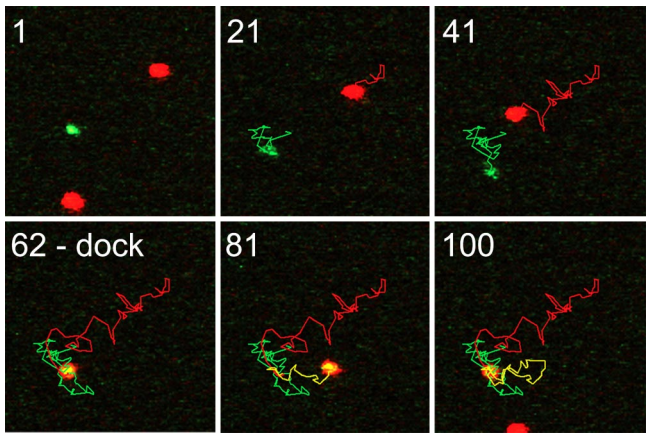

Fig. 3. Frames taken from SI Movie 1 of a docking event between an OG and a TR vesicle displaying docking oligos. Through frame 61, the vesicles diffuse independently (red and green trajectories). After docking in frame 62, the vesicles diffuse in tandem (yellow trajectory). Frames are taken at 100-ms exposure time.

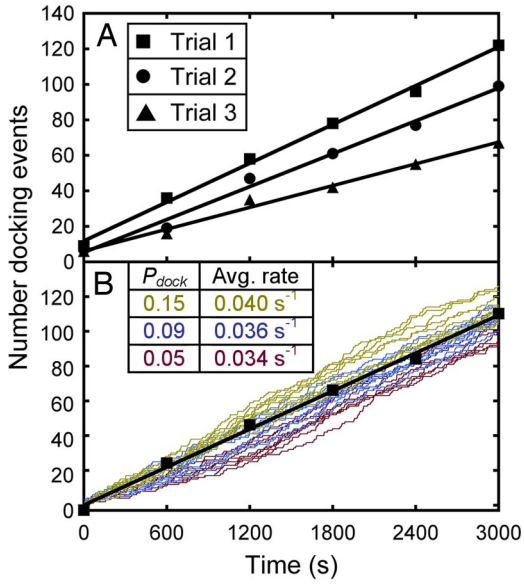

Fig. 4. Comparison of experimental and simulation time courses. (*A*) Plot of the number of docked vesicles versus time for three kinetics trials performed with vesicles labeled with an average of 10 copies of D/D′ DNA. The slope of the best linear fit for the trial 1 time course (squares) gives an effective rate of 0.036 docked vesicles per second. (*B*) Plot of simulated time courses using the initial conditions from the trial described in Fig. 4*A*. Ten time courses are plotted for $P_{dock} = 0.05$ (red), 0.09 (blue), and 0.15 (yellow). The experimental time course and fit from trial 1 (black with squares, offset to give a *y* intercept of 0) are overlaid on the simulated time courses. (*Inset*) Table gives average rates from the simulation plots for different values of P_{dock}. $P_{dock} = 0.09$ gives an average rate of 0.036 s^{-1}, which is the closest match to the experimental rate.

Table 2. Average P_{dock} values at a 90% confidence level for vesicles displaying different average copy numbers and sequences of DNA

Copy no.	C/C′	D/D′	E/E′
5	—	0.03 ± 0.02	—
10	0.002 ± 0.001	0.12 ± 0.07	0.04 ± 0.03
25	0.010 ± 0.003	>0.3*	—
50	0.06 ± 0.02	—	—

—, Combinations not studied.
*See *Discussion*.

time courses are plotted, 10 each for P_{dock} values of 0.05, 0.09, and 0.15. Fig. 4*B Inset* shows the representative simulated rates for these P_{dock} values, and the closest match to the experiment is given by $P_{dock} = 0.09$. Values for P_{dock} were extracted from at least four experimental trials using vesicles prepared with the same average number and sequence of docking DNA. Average values and standard deviations for P_{dock} for specific vesicle preparations are summarized in Table 2.

The effect of copy number on docking probability can be seen by comparing the docking probabilities for vesicles presenting the same sequences of DNA. For vesicles displaying C/C′ DNA, an overall 5-fold increase in copy number from 10 to 50 results in a 30-fold increase in reactivity. A 2-fold increase from 5 to 10 D/D′ DNA per vesicle gives a 4-fold increase in reactivity. Comparison for vesicles labeled with 25 D/D′ oligos is complicated by limitations in the kinetic analysis. Above a certain value of P_{dock} (generally ≈0.3), the representative simulated rate remains constant. Trials using vesicles labeled with 25 D/D′ oligos all give rates in this range, thus it is only possible to assign a lower limit of 0.3 to the P_{dock} value of these vesicles. In these cases, the rate of docking is limited by the incomplete mixing of nondocked vesicles rather than the reactivity of the vesicles. Docking occurs as quickly as reacted vesicles are replaced by the diffusion of nondocked vesicles from the sides of the channel. Nevertheless, the qualitative trend of increasing P_{dock} with increasing copy number of docking oligos is found for both pairs of sequences.

The docking probability also shows a strong dependence on the sequence of the complementary oligos. For vesicles labeled with D/D′ DNA [poly(A/T) sequence], the value of P_{dock} is ≈30 to 60 times greater than when using C/C′ (nonrepeating sequence). P_{dock} also is increased when using sequence E/E′ [24-mer poly(T) linker then sequence C/C′], indicating that extending the docking sequence by including a linker also can enhance docking kinetics. Vesicles labeled with noncomplementary DNA did not dock and were assigned a P_{dock} of 0. Clearly, the sequence of the oligos mediating the docking reaction plays an important role in the reactivity of vesicles.

Discussion

Docking of tethered vesicles combines two diffusion processes. First, two vesicles displaying complementary DNA sequences must diffuse across the supported lipid bilayer with $\langle D_{ves}\rangle \approx 0.2\ \mu m^2/s$ to come within a distance that allows the DNA on their surfaces to hybridize. Then, complementary docking DNAs must diffuse on the surface of the tethered vesicle, collide, and react before the vesicles move away from one another. The average diffusion constant describing DNA–lipid diffusion, $\langle D_{DNA}\rangle$, is estimated to be 1–4 $\mu m^2/s$ based on measurements of DNA–lipid conjugate diffusion in supported bilayers (26) and lipid diffusion in giant vesicles (30).

Simple lattice-diffusion simulations provide limited insight into the reasons behind the observed trends of P_{dock} based on the copy number and sequence of docking-mediating DNA. A more detailed model of the docking reaction was developed to take into account the finite size of the vesicles and the diffusion of docking DNA on the vesicles' surfaces. This model resembles somewhat the Witten and Sander model for diffusion-limited aggregation, except it analyzes the docking of pairs of particles rather than the growth of large aggregates (31). In this model (see SI Fig. 5 and *Materials and Methods*), vesicles are represented as hard spheres performing off-lattice diffusion over a supported bilayer. Vesicles display copy numbers, N_{DNA}, of docking DNA, which are represented as cylinders with radius r_{DNA} and length l_{DNA}. These cylinders undergo off-lattice diffusion over the surface of the vesicles. This model provides theoretical estimates of the scaling relationships between P_{dock} and the copy number per vesicle, N_{DNA}, and the length, l_{DNA}, of the docking sequence.

The docking probability is proportional to the cumulative overlap of cylinders on two complementary vesicles. Thus,

$$P_{dock} \propto P_{coll}\overline{T}_{ov}\overline{V}_{ov}, \qquad [1]$$

where P_{coll} is the collision probability for two vesicles, $\overline{T}_{ov}$ is the average time the vesicles are close enough so that the DNA can hybridize, which is when the surface-to-surface distance between two vesicles, d, is less than d_0, a maximum distance that depends on the length and sequence of docking DNA. Because of the diffusional motion of the vesicles, one expects $\overline{T}_{ov}$ to depend directly on d_0, which has been confirmed by simulations of vesicle diffusion (SI Fig. 6). $\overline{V}_{ov}$ is the average overlap volume between complementary DNA cylinders during this time and can be estimated by the following analytical expression:

$$\overline{V}_{ov} \approx \frac{1}{\tau}\int_0^{\tau} dt\left(\frac{4D_{DNA}t}{4\pi R^2}N_{DNA}\right)^2 \pi r_{DNA}^2(2l_{DNA}-d) \times \int d\theta_1 \int d\theta_2 \int d\varphi_1 \int d\varphi_2 v_{ov}(\theta_1, \theta_2, \varphi_1, \varphi_2). \qquad [2]$$

The angular integrals including the function v_{ov} give the overlap volume per unit length between two cylinders centered at spherical coordinates (θ_1, φ_1) and (θ_2, φ_2) on two different vesicles. The function is sharply peaked around $\theta_1 = \theta_2 = \pi/2$, $\varphi_1 = 0$, and $\varphi_1 = \pi$. The time integral describes the probability that two cylinders are at these positions and is evaluated to an upper limit of $\tau = \overline{T}_{ov}$. $4Dt$ is the area over which a docking DNA diffuses in time t. Eq. **2** is valid only for $l_{DNA} < d < 2l_{DNA}$. For $d > 2l_{DNA}$, $\overline{V}_{ov} = 0$, whereas for $d < l_{DNA}$, bending of DNA has to be taken into account, which is beyond the scope of this article.

As can be seen from Eqs. **1** and **2**, $\overline{V}_{ov}$, and therefore P_{dock}, are expected to scale as $(N_{DNA})^2$, and this finding is confirmed by Monte Carlo (MC) simulations (SI Fig. 7). Indeed, this finding agrees with the experimentally observed quadratic trends in P_{dock} with respect to N_{DNA} for C/C′ and D/D′ sequences of docking DNA, which have been studied most extensively. Because N_{DNA} describes the number of DNA on two different vesicles, this scaling is consistent with a first-order kinetic relationship between the reactivity of an individual vesicle and the number density of DNA. In this study, DNA was incorporated at a maximum number of 50 per vesicle, which gives an average of ≈600 nm^2 of surface area on the vesicle per oligo, so the DNA should be well separated (32). At higher labeling densities, crowding may begin to reduce the DNA hybridization efficiency (33). Furthermore, as N_{DNA} increases, P_{dock} will approach an upper limit of unity, so the observed first-order relationship will not be valid outside a low-density labeling regime. In these cases, more complex models of binding kinetics, such as those presented by Chesla *et al.* (34) may prove useful.

Upon inspection, Eq. **2** implies that for $\tau \cong \overline{T}_{ov}$ and $\overline{T}_{ov} \propto d_0$, $\overline{V}_{ov} \propto \overline{T}_{ov}^2 l_{DNA} \propto d_0^2 l_{DNA}$. With Eq. **1**, this gives:

$$P_{\text{dock}} \propto d_0^3 l_{\text{DNA}}. \quad [3]$$

For DNA sequences requiring full overlap, $d_0 = l_{\text{DNA}}$, so the expression reduces to $P_{\text{dock}} \propto (l_{\text{DNA}})^4$, showing that the length of the docking-mediating DNA is expected to have a large effect on the resulting reactivity of those vesicles. According to this model, three powers of this dependence are attributable to the relationship between d_0 and $\overline{T}_{\text{ov}}$. Increasing the range of separation distances that allows docking increases the time that two approaching vesicles will stay within that range. An additional power comes from the extra potential contacts that longer DNA strands have as they contact each other during the hybridization process.

The dependence of P_{dock} on d_0 and l_{DNA} is illustrated most clearly by comparing vesicles with either C/C′ or E/E′ DNA. The docking sequence is the same length for both, so l_{DNA} is effectively equivalent for the two sequences. However, the 24-bp poly(T) linkers in the E/E′ sequences allow full overlap of the docking segments at approximately three times the vesicle–vesicle separation distance as for C/C′ sequences. Thus, for C/C′ DNA, $d_0 = l_{\text{DNA}}$, whereas for E/E′ DNA $d_0 \approx 3l_{\text{DNA}}$. By Eq. **3**, this should result in a factor of 30 change in P_{dock} between these two sequences, consistent with the ≈20-fold difference found experimentally between vesicles presenting an average of 10 copies of C/C′ and E/E′ DNA (Table 2). A similar argument explains the trend in P_{dock} found between nonrepeating (C/C′) and poly(A/T) (D/D′) sequences. Because D/D′ DNA can achieve hybridization when any part of two complementary strands come into contact, d_0 describing this reaction is greater than that of C/C′ DNA, and a reasonable estimate would be twice as long. This estimate should give an ≈10-fold increase in P_{dock} from C/C′ to D/D′ DNA, which accounts for only some of the observed experimental enhancement (Table 2). The discrepancy possibly indicates that the repeating sequence relaxes constraints other than separation distances that have not been considered in the model but still are important in determining docking rates.

The high dependence of P_{dock} on l_{DNA} suggests that one way to increase the efficiency of membrane binding reactions is to increase the distance at which recognition can occur, so long as the increased length does not give rise to other effects, including interference from secondary structure or a loss in cooperativity (35). In biological systems, this effect can be achieved by increasing the length of the binding proteins. Duplication of binding motifs in binding proteins (such as found, for example, in many cadherins) could be especially effective at increasing the on-rate kinetics, although this could reduce selectivity by increasing the number of binding conformations. In the case of soluble *N*-ethylmaleimide-sensitive factor attachment protein receptors (SNAREs), the length of the proteins can be tailored via extension of the amino acid sequence. Furthermore, docking can be initiated when the ends of the proteins come into contact rather than requiring full protein overlap. This comparison is analogous to that of D/D′ and C/C′ DNA-mediated reactions and raises the possibility that the orientation of SNARE proteins enhances the docking efficiency of vesicles to the cell membrane. To conclude, tethered vesicles have been used to measure the probability and develop a simple model of DNA-mediated docking. By observing single vesicles, many future studies are possible, including finding correlations between binding and vesicle intensity (size), single-particle tracking analysis of diffusion before and after docking, and extending the system to study protein-mediated reactions and more complex reactions such as fusion.

Materials and Methods

Vesicle Preparation. Small unilamellar vesicles were formed by the extrusion method as described extensively in ref. 11. To form the supporting bilayer, 2.5 mg of egg yolk phosphatidylcholine (EYPC; Avanti) was mixed with 50 μg of 1,2-dipalmitoyl-*sn*-glycero-3-phospho-L-serine (2 mol% DPPS; Avanti Polar Lipids). For green and red fluorescently labeled vesicles, 2.5 mg of EYPC was mixed with either 73 μg of OG 1,2-dihexadecanoyl-*sn*-glycero-3-phosphoethanolamine (2 mol% OG; Invitrogen) or with 45 μg of TR 1,2-dihexadecanoyl-*sn*-glycero-3-phosphoethanolamine (1 mol% TR; Invitrogen), respectively. Chloroform was dried off under a nitrogen stream and then under vacuum. The dried lipid stocks were resuspended in 10 mM phosphate buffer, pH 7.2, containing 500 mM sodium chloride and extruded through a 0.1-μm polycarbonate filter (Whatman) to form vesicle suspensions with an average radius of 50 nm. The polydispersity as measured by dynamic light scattering was 0.04.

Stocks of DNA–lipid conjugates (12) were dissolved in a 1:1 mixture of water:acetonitrile. A volume of this solution was added to 40 μl of 10 mM phosphate buffer (containing no sodium chloride) to achieve the desired average DNA-to-vesicle ratio. Then, 10 μl of the vesicle suspensions made above were added to the diluted DNA–lipids and incubated at 4°C overnight. The final buffer composition was 10 mM phosphate, pH 7.2, containing 100 mM sodium chloride (PBS). After incorporating the DNA–lipids, the vesicles were passed through a CL-4B matrix size-exclusion column (Sigma) in PBS to separate any unincorporated DNA–lipids from the DNA-labeled vesicles. DPPS vesicles used to form the supporting bilayer were labeled with DNA of sequence A or B (see Table 1) at a ratio of three DNA per vesicle, which gave an average density of 100 DNA per square micrometer of bilayer surface area. OG and TR vesicles populations had either sequence A′ or B′ at a ratio of 0.1 DNA per vesicle to allow tethering to the supporting bilayer, which displays complementary sequence A or B. In addition, complementary sequence pairs C/C′, D/D′, or E/E′ were incorporated into OG/TR vesicles to mediate docking. Experiments were performed with vesicles displaying on average 10–50 copies of C/C′, 5–25 copies of D/D′, or 10 copies of E/E′ to study the effects of copy number and sequence of docking DNA on the docking rate of tethered vesicles. The distribution of DNAs incorporated per vesicle is expected to follow Poisson statistics.

Sample Preparation. Glass cover slides (VWR) were washed in heated detergent, thoroughly rinsed in deionized water, and then baked at 400°C for 4 h to further clean and anneal the surface. A simple three-channel microfluidic device was created by casting PDMS on a master fabricated from SU-8 on a silicon substrate. As illustrated in Fig. 2*A*, three inputs and one output create three-lane, laminar flow during vesicle deposition. Then, 25 g of PDMS monomer and 2.5 g of curing agent (Slygard 184) were thoroughly mixed, degassed under vacuum, cast onto the master, and incubated at 80°C for 1 h to polymerize the PDMS. Holes were punched in individual devices to create the input and output ports, the device was treated in a plasma cleaner (Harrick) to oxidize the PDMS, and the PDMS channel was bonded to a clean glass cover slide to create a flow channel.

DPPS vesicles displaying tethering oligo A (or B) in PBS were added to the flow channel and allowed to incubate with the glass substrate for 15 min. Vesicle fusion to the glass formed a supported bilayer displaying oligo A covering the entire surface within the flow channel. Excess vesicles then were washed away by flowing fresh PBS through the channel, and the central input port was left filled with clean buffer. Solutions containing OG and TR vesicles labeled with at most 1 oligo for tethering (sequence A′ or B′) and variable copies for docking (C/C′, D/D′, or E/E′) were added to the two outer input ports, creating three-lane flow in the channel. Steady flow was maintained manually for 40 min to allow tethering of the red and green vesicles to the supported bilayer in the channel. Once tethering was completed, the channel again was washed with fresh PBS before imaging.

Image Acquisition. Epifluorescence microscopy of samples was performed on a Nikon TE300 inverted microscope with a mercury arc lamp light source and 100× oil-immersion objective (N.A. =

1.45). A two-color imaging device (Optical Insights) was used to separate TR and OG emission and place them on two halves of a Cascade 650 electron multiplying charge-coupled device (EM-CCD) detector (Photometrics). Acquired images thus were a composite of two half images, so they were separated, aligned, false-colored, and overlaid with MetaMorph processing software (Universal Imaging). Initial image alignment was performed by using dual-fluorescence beads and did not change over the course of experiments.

In kinetics trials, after vesicle tethering and washing, the flow channel was imaged on the microscope, and the edge of the channel was located. The inverted geometry of the microscope allowed imaging to be performed through the glass substrate, therefore avoiding background from vesicles deposited on the ceiling of the flow channel. A 1-s video was taken at this location at a rate of 100 ms per frame. Then the stage was moved one frame width over ($\approx$25 μm), and another video was taken. This process was repeated to create a lateral cross-section of the channel for a single time point in the course of the experiment. Time points were taken at 10-min intervals for up to 1 h to follow the progression of the reaction.

Diffusion Simulations. The following simulations have been performed to model the docking reaction of tethered vesicles: (*i*) lattice diffusion of vesicles, (*ii*) off-lattice diffusion of vesicles, and (*iii*) off-lattice diffusion of DNA tethers.

(i) Lattice diffusion of vesicles. Diffusion of vesicles tethered to a supported lipid bilayer was modeled *in silico* by particles performing random motion on a square lattice. Typically, each lattice site represents a bilayer patch of size $(\Delta l)^2 = (0.2\ \mu\text{m})^2$, giving average simulation dimensions of 750 $\times$ 180 steps corresponding to an observed, experimental cross-section of 150 $\times$ 35 μm. Reflecting boundaries were implemented at the left and right sides of the simulation corresponding to the walls of the flow chamber where tethered vesicles were observed to reflect. Periodic boundaries were implemented at the top and bottom sides of the lattice (normal to the direction of flow in the channel).

Initial vesicle positions were determined from the first cross-section taken in an experimental kinetics trial with the aid of MetaMorph. First, an intensity threshold was applied to filter out background signal. Then, discrete collections of pixels above the threshold were identified as vesicles and checked visually. Lastly, coordinates of these objects were converted and exported for use in the simulation.

Diffusional motion [with the experimentally observed diffusion coefficient $\langle D_{\text{ves}}\rangle \approx 0.2\ \mu\text{m}^2/\text{s}$ (26)] is implemented by self-avoiding random motion of the vesicles on the lattice. Once per time step (corresponding to a real time interval $\Delta t = 50$ ms), vesicles moved one lattice site either up, down, left, or right provided that the new site was unoccupied. If it was occupied, the corresponding vesicles were considered to have collided. These events were given a probability of docking, P_{dock}, upon which the vesicles involved were removed from the simulation. Otherwise, the vesicles continued to diffuse with the next time step.

(ii) Off-lattice diffusion of vesicles. Here, $n = 10$ (nonlabeled) vesicles of radius R tethered to a supported bilayer performed random motion in a box of size $L_x \times L_y$ (with $L_x/R = L_y/R = 10$) with reflecting walls. Vesicles were assumed to carry DNA tethers of length l_{DNA}. Once per time step, vesicles moved a distance $\Delta l/R = 0.01$ in a random direction provided no collision occurred during motion. The center-to-center distances, d, between all vesicle pairs were measured. If two vesicles were close enough so that their DNA tethers could overlap (i.e., $d < d_0$), the overlap time was measured (i.e., the number of time steps for which $d < d_0$). The average overlap time was measured by averaging over 10^7 MC steps for different values of d_0. For vesicles with $R = 50$ nm and diffusion coefficient $\langle D_{\text{ves}}\rangle = 0.2\ \mu\text{m}^2/\text{s}$, one MC step corresponds to 10 ns.

(iii) Off-lattice diffusion of DNA tethers. Diffusion of DNA tethers on spherical vesicles was simulated. Two vesicles of radius R were kept at fixed distance d (with $d < d_0$). Tethers were modeled as cylinders of radius r_{DNA} and length l_{DNA} to represent the volume in which the tethers on two vesicles can interact. Diffusion was implemented as movement in a random direction with one step (of size 0.01 R) occurring per time step. For simplicity, self-avoidance of the tethers was not taken into account. During the simulation the overlap volume between all cylinders was calculated as a function of time.

We thank Gregory Miller and Bettina van Lengerich for assistance in synthesizing the DNA–lipid conjugates. This work was supported in part by grants from the National Science Foundation Biophysics Program, National Institutes of Health Grant GM069630, and the Materials Research Science and Engineering Centers (MRSEC) Program of the National Science Foundation under Award DMR-0213618 (Center on Polymer Interfaces and Macromolecular Assemblies). P.L. acknowledges support from the German Academic Exchange Service (DAAD).

1. Gumbiner BM (1996) *Cell* 84:345–357.
2. Dustin ML, Bivona TG, Philips MR (2004) *Nat Immun* 5:363–372.
3. Weber T, Zemelman BV, McNew JA, Westermann B, Gmachl M, Palati F, Söllner T, Rothman JE (1998) *Cell* 92:759–772.
4. Schuette CG, Hatsuzawa K, Margittai M, Stein A, Riedel D, Küster P, König M, Seidel C, Jahn R (2004) *Proc Natl Acad Sci USA* 101:2858–2863.
5. Dennison SM, Bowen ME, Brunger AT, Lentz BR (2006) *Biophys J* 90:1661–1675.
6. Chen X, Araç D, Wang T-M, Gilpin CJ, Zimmerberg J, Rizo J (2006) *Biophys J* 90:2062–2074.
7. Fix M, Melia TJ, Jaiswal JK, Rappoport JZ, You D, Söllner TH, Rothman JE, Simon SM (2004) *Proc Natl Acad Sci USA* 101:7311–7316.
8. Bowen ME, Weninger K, Brunger AT, Chu S (2004) *Biophys J* 87:3569–3584.
9. Liu T, Tucker WC, Bhalla A, Chapman ER, Weisshaar JC (2005) *Biophys J* 89:2458–2472.
10. Groves JT, Dustin ML (2003) *J Immunol Methods* 278:19–32.
11. Yoshina-Ishii C, Boxer SG (2003) *J Am Chem Soc* 125:3696–3697.
12. Yoshina-Ishii C, Miller GP, Kraft ML, Kool ET, Boxer SG (2005) *J Am Chem Soc* 127:1356–1357.
13. Brian AA, McConnell HM (1984) *Proc Natl Acad Sci USA* 81:6159–6163.
14. Groves JT, Boxer SG (2002) *Acc Chem Res* 35:149–157.
15. Wagner ML, Tamm LK (2000) *Biophys J* 79:1400–1414.
16. Naumann CA, Prucker O, Lehmann T, Rühe J, Knoll W, Frank CW (2002) *Biomacromolecules* 3:27–35.
17. Tanaka M, Sackmann E (2005) *Nature* 427:656–663.
18. Atanasov V, Knorr N, Duran RS, Ingebrandt S, Offenhäusser A, Knoll W, Köper I (2005) *Biophys J* 89:1780–1788.
19. Valincius G, McGillivray DJ, Febo-Ayala W, Vanderah DJ, Kasianowicz JJ, Lösche M (2006) *J Phys Chem B* 110:10213–10216.
20. Johnson JM, Ha T, Chu S, Boxer SG (2002) *Biophys J* 83:3371–3379.
21. Boukobza E, Sonnenfeld A, Haran G (2001) *J Phys Chem B* 105:12165–12170.
22. Okamus B, Wilson TJ, Lilley DMJ, Ha T (2004) *Biophys J* 87:2798–2806.
23. Patel AR, Frank CW (2006) *Langmuir* 22:7587–7599.
24. Yoon T-Y, Okumus B, Zhang F, Shin Y-K, Ha T (2006) *Proc Natl Acad Sci USA* 103:19731–19736.
25. Indriati P, Höök F (2004) *J Am Chem Soc* 126:10224–10225.
26. Yoshina-Ishii C, Chan Y-HM, Johnson JM, Kung LA, Lenz P, Boxer SG (2006) *Langmuir* 22:5682–5689.
27. Kam L, Boxer SG (2000) *J Am Chem Soc* 122:12901–12902.
28. Kam L, Boxer SG (2003) *Langmuir* 19:1624–1631.
29. Ajo-Franklin C, Yoshina-Ishii C, Boxer SG (2005) *Langmuir* 21:4976–4983.
30. Scwhille P, Korlach J, Webb WW (1999) *Cytometry* 36:176–182.
31. Witten TA, Jr, Sander LM (1981) *Phys Rev Lett* 47:1400–1403.
32. Steel AB, Herne TM, Tarlov MJ (1998) *Anal Chem* 70:4670–4677.
33. Peterson AW, Heaton RJ, Georgiadis R (2000) *J Am Chem Soc* 122:7837–7838.
34. Chesla SE, Selvaraj P, Zhu C (1998) *Biophys J* 75:1553–1572.
35. Lytton-Jean AKR, Mirkin C (2005) *J Am Chem Soc* 127:12754–12755.